Boundary of prewetting transition of Ar on a Li surface

Ming Zeng, Jianguo Mi,* and Chongli Zhong
Laboratory of Computational Chemistry, Department of Chemical Engineering, Beijing University of Chemical Technology, Beijing 100029, China

(Received 21 July 2010; published 29 September 2010)

The prewetting transition of Ar adsorbed on a planar structureless Li surface was investigated using the density-functional theory, In the theoretical model, the renormalization-group transform and the three-body intermolecular interactions were considered. To describe the thermodynamic properties of Ar, a reliable *ab initio* potential was applied to model the interactions between Ar atoms and Li surface. The thin-film-thick-film coexistence diagram for prewetting transition was calculated. The prewetting critical temperature (upper boundary of prewetting transition) is found to be lower than those previous predictions. With the difference of thickness between the thin and the thick films served as the order parameter, the predicted prewetting critical exponent β is 0.175 ± 0.018. The value is close to the two-dimensional Ising value, demonstrating the predicted upper boundary is reliable. The wetting temperature (lower boundary of prewetting transition) was determined by two different methods: extrapolation of the chemical difference and evaluation of the contact angle via Young's equation, and nearly the same results are obtained. The convergence of the two methods further validates that the lower boundary is also correct. The wetting temperature is also found to be lower than those previous predictions.

DOI: 10.1103/PhysRevB.82.125452 PACS number(s): 68.08.Bc, 61.20.Ne, 64.70.F−, 68.65.−k

I. INTRODUCTION

Fluids restricted to solid substrates exhibit a variety of properties that differ substantially from those of bulk fluids.[1,2] A deep understanding of the surface phenomena is of considerable importance for scientific researches and industrial processes. Prewetting transition represents one of these surface phenomena. The first sketches of prewetting transition were brought forward simultaneously by Cahn[3] and Ebner and Saam[4] in theoretical treatments. The phenomenon was investigated by experiment for some systems, such as He on Cs,[5] H_2 on Rb,[6] and mercury on sapphire.[7] In the last few decades, a large number of studies have been carried out to achieve a better understanding of the phenomenon using different theoretical and simulation techniques.[8–21] Although considerable progress has been made,[22–24] the exact region in which the prewetting transition for a given system can be found is still in dispute, such as Ar on alkali-metal surfaces.[14,15,20]

With a substrate potential of moderate strength, the prewetting transition corresponds to a jump from a thin adsorbed film to a thick adsorbed film at the surface when the pressure P (or chemical potential μ) is below the bulk vapor-liquid saturation pressure P_{sat} (or chemical potential μ_{sat}). The boundary of the prewetting transition originates at a first-order wetting transition at the wetting temperature T_w and terminates at the prewetting critical temperature T_{pwc}.

Critical temperature is one of the most important characteristics of confined fluids. Experiment revealed that the critical temperature of confined fluids differs substantially from those of the corresponding bulk systems.[25] Nakanishi and Fisher[26] conjectured that the prewetting critical point should display two-dimensional (2D) Ising-type criticality on the basis of Landau phenomenological theory. Nicolaides and Evans[27] confirmed the conjecture via Monte Carlo simulation of a three-dimensional lattice-gas model. The coarse-grained method, however, may not be appropriate for realistic continuum fluids. Errington and Wilbert[18] evaluated the prewetting boundary tensions through a combination of finite-size scaling and grand canonical Monte Carlo simulation. They obtained a lower prewetting critical temperature than that from the simulation without finite scaling.[17]

On the other hand, Ancilotto and Toigo,[14] Sartarelli and Szybisz[19,20] have successively studied the adsorption of Ar and Ne on planar substrates of alkali metals using a mean-field density-functional theory (DFT). To reproduce the experimental phase coexistence curve as well as the critical point of bulk fluids, Sartarelli and Szybisz employed three adjustable parameters to describe the intermolecular interactions. Although the theoretical model gives the correct critical point of bulk fluids, it might not be appropriate to be extended to predict the critical prewetting temperature of confined fluids since the two kinds of exponent law for bulk and confined fluids are quite different. In other words, the mean-field density-functional model cannot predict the 2D Ising-type criticality of prewetting. Accordingly, the accuracy of those prewetting transition boundaries is questionable. When temperature approaches the critical region, the density distribution is increasingly inhomogeneous or the density fluctuation wavelength is increasingly long ranged to the critical point. This kind of density fluctuation needs to be considered with a special treatment such as the renormalization-group (RG) transform,[28,29] which has become central to any discussion of critical phenomena.

In this work, we applied our recently developed density-functional model[30] to investigate the wetting and prewetting transition of Ar adsorbing on a Li surface. The well addressed modified fundamental measurement theory[31,32] was adopted to describe the hard sphere reference term. For attractive part, the free-energy functional was constructed in a weighted density approximation,[30] and the free energy associated with the three-body interaction was included. Furthermore, the long-range density fluctuation near the critical re-

gion was considered by the confined RG transform.[30] We constructed our confined RG transform on the basis of the density functional by sharing the same direct correlation function (DCF), keeping the theoretical crossover in self-consistency both inside and outside of the critical region.

II. THEORY

As a spherical symmetric fluid, Ar can be adequately described by the two-body intermolecular potential together with the three-body intermolecular potential. The two-body interaction is given by the Lennard-Jones (LJ) potential

$$\varphi_2(r) = 4\varepsilon\left[\left(\frac{\sigma}{r}\right)^{12} - \left(\frac{\sigma}{r}\right)^{6}\right], \tag{1}$$

where $\varepsilon/k_B = 119.4$ K is the energy parameter, k_B is the Boltzmann constant, and $\sigma = 3.36$ Å is the soft diameter. The split between the repulsion and attraction for the LJ potential can be made with an effective hard-sphere diameter[33,34]

$$d = \frac{1 + 0.2977T^*}{1 + 0.33163T^* + 0.00104771T^{*2}}\sigma, \quad T^* = \frac{k_B T}{\varepsilon}, \tag{2}$$

where T is the absolute temperature. The effect of three-body interaction can be described by the following potential:[35]

$$\varphi_3(r_1, r_2, r_3) = \frac{\nu(1 + 3\cos\theta_1\cos\theta_2\cos\theta_3)}{(r_1, r_2, r_3)^3}, \tag{3}$$

where r_1, r_2, r_3, θ_1, θ_2, and θ_3 are the sides and interior angles of the triangle formed by the molecules 1, 2, 3 and ν is the interaction coefficient, which is known to be 73.2×10^{-84} erg cm^9 for Ar.[35]

For adsorption of Ar on planar structureless substrates of alkali metals, the interaction V_{ext} between Ar atoms and a wall of Li separated by a distance z is given by the *ab initio* potential of Chizmeshya *et al.*[36]

$$V_{ext}(z) = V_0(1 + \alpha z)e^{-\alpha z} - f_2[\beta(z)(z - z_{vdW})]\frac{C_{vdW}}{(z - z_{vdW})^3} \tag{4}$$

where V_0 is amplitude, α is an exponent, C_{vdW} and z_{vdW} are the strength and reference plane position of the van der Waals potential, respectively. $f_2(x) = 1 - e^{-x}(1 + x + x^2/2)$ is a damping function which accounts for the effect of atom-substrate wave function overlap on the van der Waals correlation energy, $\beta(z) = \alpha^2 z/(1 + \alpha z)$ is an alternative spatially dependent damping parameter. The model parameters V_0, α, C_{vdW}, and z_{vdW} for Ar interacting with Li can be found in Table I of Ref. 36.

To describe the adsorption of Ar on the wall of Li, the density distribution of Ar needs to be obtained. The DFT is readily available to deal with this problem. For inhomogeneous fluids, the essential task of the DFT is to derive an analytical expression for the grand potential $\Omega[\rho(\mathbf{r})]$, or equivalently, the intrinsic Helmholtz free energy $F[\rho(\mathbf{r})]$, $F[\rho(\mathbf{r})] = \int d\mathbf{r} f[\rho(\mathbf{r})]$, as a functional of density distribution. Within the grand canonical ensemble, the grand potential relates the intrinsic free energy by

$$\Omega[\rho(\mathbf{r})] = k_B T\int d\mathbf{r}\rho(\mathbf{r})\{\ln[\rho(\mathbf{r})\Lambda^3] - 1\} + F_{rep}[\rho(\mathbf{r})] + F_{att}[\rho(\mathbf{r})] + \delta F_{RG}(\rho_{av}) + \int d\mathbf{r}\{\rho(\mathbf{r})[V_{ext}(\mathbf{r}) - \mu]\}, \tag{5}$$

where $\rho(\mathbf{r})$ denotes the density distribution with configuration $\mathbf{r}$, $\Lambda = \sqrt{2\pi m k_B T/h^2}$ is the thermal de Broglie wavelength, ρ_{av} is the average density of fluids restricted to surface, which will be defined later, $F_{rep}[\rho(\mathbf{r})]$ stands for the hard-sphere reference system, $F_{att}[\rho(\mathbf{r})]$ accounts for the attractive interactions, $\delta F_{RG}(\rho_{av})$ represents the contribution from the confined RG transform of the long-range density fluctuations, $V_{ext}(\mathbf{r})$ is the potential of substrate, and μ is the chemical potential of bulk fluids.

The hard-sphere functional $F_{rep}[\rho(\mathbf{r})]$ can be described by

$$F_{rep}[\rho(\mathbf{r})] = k_B T\int d\mathbf{r}\left\{-n_0\ln(1 - n_3) + \frac{n_1 n_2 - \mathbf{n}_{V1}\mathbf{n}_{V2}}{1 - n_3} + \frac{1}{36\pi}\left[n_3\ln(1 - n_3) + \frac{n_3^2}{(1 - n_3)^2}\right]\frac{n_2^3 - 3n_2\mathbf{n}_{V1}\mathbf{n}_{V2}}{n_3^3}\right\}, \tag{6}$$

where n_0, n_1, n_2, n_3 are the scalar-weighted densities and the boldface symbols $\mathbf{n}_{V1}, \mathbf{n}_{V2}$ are the vector-weighted densities. They are defined by

$$n_\alpha(\mathbf{r}) = \int \rho(\mathbf{r}')w^{(\alpha)}(\mathbf{r} - \mathbf{r}')d\mathbf{r}', \tag{7}$$

where the weighted functions $w^{(\alpha)}(r)$, $\alpha = 0, 1, 2, 3, V1, V2$ are expressed in terms of the Heaviside step function $H(r)$ and the Dirac delta function $\delta(r)$ by

$$w^{(2)}(\mathbf{r}) = \pi d^2 w^{(0)}(\mathbf{r}) = 2\pi d w^{(1)}(\mathbf{r}) = \delta(d/2 - r), \tag{8}$$

$$w^{(3)}(\mathbf{r}) = H(d/2 - r), \tag{9}$$

$$w^{(V2)}(\mathbf{r}) = 2\pi d w^{(V1)}(\mathbf{r}) = \frac{\mathbf{r}}{r}\delta(d/2 - r). \tag{10}$$

For the attractive part, weighted density approximation[37] can be employed to account for attractive contribution. In this case, $F_{att}[\rho(\mathbf{r})]$ can be expressed as

$$F_{att}[\rho(\mathbf{r})] = \int \rho(\mathbf{r})a_{att}[\bar{\rho}(\mathbf{r})]d\mathbf{r}, \tag{11}$$

$$\bar{\rho}(\mathbf{r}) = \int \rho(\mathbf{r}')\omega_{att}(|\mathbf{r} - \mathbf{r}'|)d\mathbf{r}', \tag{12}$$

$$\omega_{att}(r) = \frac{c_{att}(r)}{\int c_{att}(r)d\mathbf{r}} \tag{13}$$

in which a_{att} is the free energy per particle from attractive contribution, $\bar{\rho}(\mathbf{r})$ is the weighted density, $\omega_{att}(r)$ is the weight function, and $c_{att}(r)$ is the DCF of the bulk fluids from attractive contribution. Similar to Lee and Barker,[38] the

free energy from attractive contribution a_{att} can be given by a sum of perturbation terms for bulk fluids

$$a_{att} = a_1 + a_2, \tag{14}$$

$$a_1 = 2\pi\rho \int_\sigma^\infty g(r)\varphi_2(r)r^2 dr, \tag{15}$$

$$a_2 = \frac{\rho^2}{6}\int_V \int_V \varphi_3(r_1,r_2,r_3)g(r_1)g(r_2)g(r_3)d\mathbf{r}_2 d\mathbf{r}_3, \tag{16}$$

where $g(r)$ is the radial distribution function (RDF) for bulk fluids. Recently, a satisfactory analytical solution for RDF of LJ fluids was given by the first-order mean spherical approximation (FMSA).[39] The accurate RDF for LJ fluids can be further improved by combining FMSA with the simplified exponential approximation[39,40]

$$g(r) = g_0(r)\exp[g_1(r)] \tag{17}$$

and

$$rg_0(r) = \sum_{n=0}^{\infty} (-12\eta)^n C(1,n+1,n+1,r-n-1), \tag{18}$$

$$rg_1(r) = \beta\varepsilon k_1 \frac{(1-\eta)^4}{Q^2(z_1)}\sum_{n=0}^{\infty}(1+n)(-12\eta)^n D(6,n,n+2,z_1,r-n-1) - \beta\varepsilon k_2 \frac{(1-\eta)^4}{Q^2(z_2)}\sum_{n=0}^{\infty}(1+n)(-12\eta)^n D(6,n,n+2,z_2,r-n-1), \tag{19}$$

where $\beta = 1/k_B T$, $\eta = \frac{1}{6}\rho\pi d^3$ is the packing factor, the coefficients k_1, k_2, z_1, z_2, $1/Q^2(z)$, $C(n_1,n_2,n_3,r)$, and $D(n_1,n_2,n_3,z,r)$ are well documented.[30,39,40] In Eq. (13), the DCF of the bulk fluids from attractive contribution $c_{att}(r)$ is defined as the difference between the total DCF and the hard sphere DCF, $c_{att}(r) = c(r) - c_{hs}(r)$, with $c_{hs}(r)$ given by[41]

$$c_{hs}(r) = \begin{cases} -\dfrac{\eta(1+2\eta)^2}{2(1-\eta)^4}r^3 + \dfrac{6\eta(1+\eta+\eta^2/4)}{(1-\eta)^4}r - \dfrac{(1+2\eta)^2}{(1-\eta)^4}, & r < 1 \\ 0, & r > 1. \end{cases} \tag{20}$$

While the total DCF $c(r)$ relates to the total correlation function $h(r)$, or the RDF $g(r) = h(r) + 1$ through the Ornstein-Zernike equation

$$\tilde{h}(k) = \tilde{c}(k) + \rho\tilde{h}(k)\tilde{c}(k), \tag{21}$$

where circumflex stands for the Fourier transform. Thus, the total DCF $c(r)$ can be obtained using the RDF from Eq. (17) as input. The superiority of the improved DCF has been stated in our recent paper.[42]

For prewetting transition, it has been well addressed[26,27] that the prewetting critical point is a 2D Ising critical point as prewetting is in analogous to a vapor-liquid phase transition in 2D. Therefore, it is necessary to consider the 2D density fluctuation near the prewetting critical point. This long-range density fluctuation can be remedied with our confined RG transform[30]

$$f_n(\rho_{av}) = f_{n-1}(\rho_{av}) + \delta f_{RG,n}(\rho_{av}), f_0(\rho_{av}) = f_{ref}(\rho_{av}), \tag{22}$$

$$\delta f_{RG,n}(\rho_{av}) = -\frac{1}{\beta A_n}\ln\left[\frac{\int_0^{\rho_{av}} dx \exp\{-A_n[\beta f_{n-1,D}(\rho_{av},x) + 2\pi C_{4,att}x^2k_n^2 - 2\pi C_{6,att}x^2k_n^4]\}}{\int_0^{\rho_{av}} dx \exp\{-A_n[\beta f_{n-1,D}(\rho_{av},x) + 2\pi C_{2,att}x^2]\}}\right], \tag{23}$$

$$f_{n-1,D}(\rho_{av},x) = \frac{f_{n-1}(\rho_{av}+x) + f_{n-1}(\rho_{av}-x)}{2} - f_{n-1}(\rho_{av}), \tag{24}$$

$$C_{n,att}(r) = \frac{1}{(n-1)!}\int_0^\infty c_{att}(r)r^n d\mathbf{r}. \tag{25}$$

The average area of the fluctuation plane A_n used in Eq. (23) are chosen to be a function of wavelength $A_n = (\lambda_n)^2$ with $\lambda_n = 3^{n-1}\lambda_1$. The initial wavelength λ_1 is assumed to be 4σ. In later transforms, the fluctuation magnitude in the density wave planes is increased by $k_n = k_1/3^{n-1}$ with $k_1 = 2\pi/\lambda_1$. In Eqs. (22)–(24), ρ_{av} is the reference density for the RG transform, which employs the value of the average density of fluids restricted to surface

$$\rho_{av} = (1/l_s)\int_0^{z_m} \rho(z)dz, \tag{26}$$

where $l_s = z_m dz$, z_m is the end point of the integration range.

The point can be selected by the following procedure: span the density profile from right to left, mark the point (+) whose second order derivative of $\rho(z)$ with respect to z equals zero, as shown in Fig. 1. This is because the point is the inflection point to distinguish the surface from bulk areas. It is the surface fluid rather than the bulk fluid need the RG transform.

The reference free-energy density f_{ref} is given by $f_{\mathrm{ref}}=\rho_{\mathrm{av}}(a_{\mathrm{id}}+a_{\mathrm{hs}}+a_{\mathrm{att}})$. The free energy per particle of ideal part $a_{\mathrm{id}}=\ln(\rho_{\mathrm{av}}\Lambda^3)-1$. The free energy per particle from hard-sphere contribution is $a_{\mathrm{hs}}=(4\eta-3\eta^2)/(1-\eta)^2$. The attractive term a_{att} is the same as in Eq. (14). After several times of iteration, the free energy due to long-range density fluctuation can be incorporated into the short-range contribution, and the density profile can be obtained.

Combining DFT with the confined RG transform, we can calculate the final density distribution by minimizing the grand potential

$$\rho(\mathbf{r})=\begin{cases}\exp\left(\beta\mu-\beta\dfrac{\delta\{F_{\mathrm{hs}}[\rho(\mathbf{r})]+F_{\mathrm{att}}[\rho(\mathbf{r})]\}}{\delta\rho(\mathbf{r})}-\beta\dfrac{\delta[\delta F_{\mathrm{RG}}(\rho_{\mathrm{av}})]}{\delta\rho_{\mathrm{av}}}-\beta V_{\mathrm{ext}}(\mathbf{r})\right), & z<z_{\mathrm{m}}\\ \exp\left(\beta\mu-\beta\dfrac{\delta\{F_{\mathrm{hs}}[\rho(\mathbf{r})]+F_{\mathrm{att}}[\rho(\mathbf{r})]\}}{\delta\rho(\mathbf{r})}-\beta V_{\mathrm{ext}}(\mathbf{r})\right), & z>z_{\mathrm{m}}.\end{cases} \tag{27}$$

In Eq. (27), one can find that the confined RG transform is only added in the range near to the surface ($z<z_{\mathrm{m}}$). The local-density distribution $\rho(\mathbf{r})$ can be calculated with an iteration procedure. The initial local-density profiles and the average densities can be calculated without the confined RG transform. Based on the average densities, the confined RG recursions can be performed and added, and the next density profiles are recalculated with the DFT with confined RG transform. The iterations are performed until the grand potential achieves a minimum.

To investigate the lower boundary of prewetting transition, the wetting temperature of the system needs to be determined. Young's equation provides a simple description of wetting transition in terms of the surface tensions of different interfaces. This kind of transition has been studied extensively to evaluate the contact angle for fluid-wall system[43] via Young's equation

$$\cos\theta=\frac{\gamma_{\mathrm{vw}}-\gamma_{\mathrm{lw}}}{\gamma_{\mathrm{vl}}}, \tag{28}$$

where θ is the contact angle, γ_{vl}, γ_{vw}, and γ_{lw} denote the surface tension of the vapor-liquid, vapor-wall, and liquid-wall interface, respectively. For fluid wetting on the substrate with the given potential $V_{\mathrm{ext}}(z)$, γ_{vl}, γ_{vw}, and γ_{lw} are calculated under the vapor-liquid saturation pressure P_{sat}

$$\gamma_{\mathrm{vl}}=\int_0^\infty[f[\rho(z)]-\rho(z)\mu_{\mathrm{sat}}+P_{\mathrm{sat}}]dz \tag{29}$$

and

$$\gamma_{\mathrm{vw,lw}}=\int_0^\infty[f[\rho(z)]-\rho(z)\mu_{\mathrm{sat}}+\rho(z)V_{\mathrm{ext}}(z)+P_{\mathrm{sat}}]dz. \tag{30}$$

At different temperatures, the contact angle can vary from complete drying ($\cos\theta=-1$) to partial wetting ($\cos\theta<1$), and finally to complete wetting at the wetting temperature T_{w}, at which $\cos\theta=1$ is first realized.

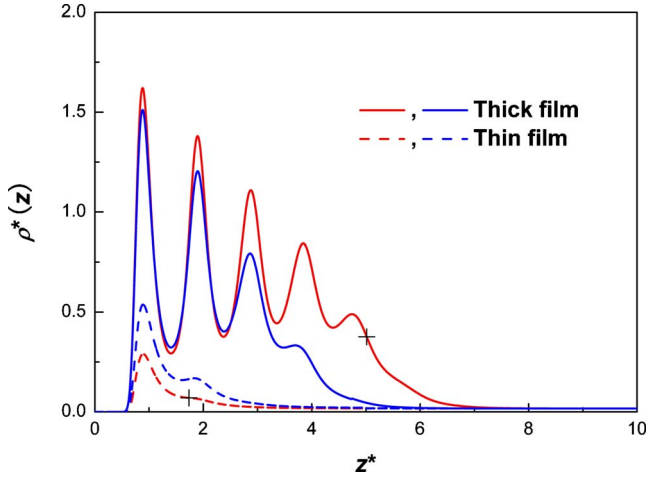

FIG. 1. (Color online) Equilibrium density profiles at $T^*=0.920$. The blue (without the markers) and red (with the markers) lines correspond to the density profiles obtained with and without the confined RG transform, respectively. The markers + represent the end points of the range in which the density profile is averaged to obtain ρ_{av}.

III. RESULTS AND DISCUSSION

As a typical example, the system of Ar adsorption on a Li surface was studied. A series of calculations were performed to determine the wetting and prewetting properties such as wetting temperature, prewetting critical temperature, and prewetting critical exponent. Throughout the whole calculations, no adjustable parameter was adopted.

Prewetting transition is usually characterized by the coexistence between thin and thick substrate films at a constant pressure (chemical potential). To draw the thin-film-thick-film coexistence diagram, it is necessary to get equilibrium

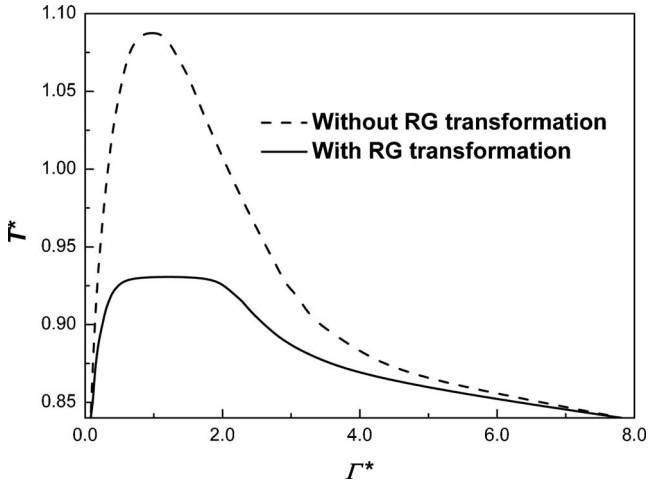

FIG. 2. Prewetting coexistence curve. The solid and dash lines represent the results with and without the confined RG transform, respectively.

density profiles at different temperatures. The numerical implements were performed via Eq. (27). To illustrate the role of the RG transform, two sets of the density profiles were calculated using the DFT without and with the RG transform, respectively. Examples of the density profiles of the thin and the thick films at $T^*=0.920$ are displayed in Fig. 1, without and with the RG transform. The difference between the two sets of profiles is quite obvious. For density profile corresponding to the thick film obtained without the RG transform, there are four peaks whose maximum value is higher than the bulk density of liquid Ar $\rho^*=0.6998$ at $T^*=0.920$. With the RG transform, the number of the peaks decreases to three. As for the thin film, both the density profiles in Fig. 1 do not extend beyond a couple of molecular diameters from the surface. The density of the first peak with the RG transform, however, is higher than the one without the RG transform. It is shown that the RG transform makes the difference between the thin and the thick films smaller at a given temperature, which means that the original phase diagram given by the DFT without the RG transform is suppressed. The smaller phase loop finally leads to a lower prewetting critical temperature or the upper boundary of the prewetting transition. Accordingly, density profiles at various temperatures were calculated. The coverage of either the thin film or the thick film at the substrate surface can be obtained from the density $\rho(z)$ via

$$\Gamma = \int_0^\infty [\rho(z) - \rho_v] dz, \tag{31}$$

where ρ_v is the density of the vapor phase coexisting with the adsorbed fluid. The thin-film-thick-film coexistence curve for prewetting transition is depicted in Fig. 2. Without the RG transform, the prewetting critical temperature is $T^*_{pwc}=1.087$, corresponding to the real temperature $T_{pwc}=129.788$ K. This value is nearly the same as that predicted by Ancilotto and Toigo[14] with $T_{pwc}=130$ K. In their DFT calculation, there are two parameters need to be set down to reproduce the experimental values of the bulk liquid and vapor densities at coexistence, and the values of the parameters vary with the temperatures. Later, Sartarelli and Szybisz[20] introduced a third free parameter to account for residual interactions near the critical point and obtained a lower prewetting critical temperature $T_{pwc}=119$ K. Due to a better reproduction of critical point of bulk Ar,[20] the result is better than those given by Ancilotto and Toigo.[14] The lower T_{pwc} comes from the three adjustable parameters.[20] The mean-field nature of the model, however, cannot describe the 2D density fluctuations since the 2D characteristic of the prewetting critical point are not included in their approach. It was well addressed[26,27] that the prewetting critical point is in dimension d-1 (d is the bulk dimensionality), so the 2D density fluctuations should be of considerable influence on determination of the prewetting critical temperature. By introducing the RG transform, we recalculated the prewetting coexistence and obtained a lower prewetting critical temperature $T^*_{pwc}=0.931$, corresponding to the real temperature $T_{pwc}=111.161$ K. As shown in Fig. 2, the exaggerated critical loop given by DFT without the RG transform is successfully suppressed by the DFT with the RG transform. Figure 2 also shows that, when the temperature decreases gradually from the prewetting critical temperature, the coexistence curve obtained with the RG transform recovers to the data obtained without the RG transform. This recovery indicates that the RG transform has little effect if the temperature is far from the prewetting critical temperature. Hence, the theoretical crossover is self-consistent. To further validate the reliability of the prewetting critical temperature obtained with the RG transform, the criticality of prewetting transition was analyzed and the critical exponent was derived. In this case, the difference of thickness between the thin and the thick films is served as the order parameter which vanishes at T^*_{pwc}. The jump in thickness relates to the temperature with the scaling law

$$\Delta\Gamma^* \propto (T^*_{pwc} - T^*)^\beta, \tag{32}$$

where β is the critical exponent. Figures 3 and 4 present the order parameter and the fitting lines for prewetting curves without and with the RG transform, respectively. The slopes of the plots denote the values of β. It can be found from the two figures that the order parameter obey the scaling law if the temperature is not far from T^*_{pwc}. Far from T^*_{pwc}, the order parameter gradually deviate the fitting lines. This phenomenon is foreseeable since the thickness of the thick film will diverge if the temperature is down to the wetting temperature, indicating that the wetting transition has an influence on the prewetting criticality, and that the scaling law for prewetting criticality should limit to a finite range. Therefore, we determined the exponent for prewetting curves without and with the RG transform in the range of $T^*_{pwc}-T^*=0.1$ and $T^*_{pwc}-T^*=0.02$, respectively. For the curve without the RG transform, the critical exponent is $\beta=0.542\pm0.011$, close to 1/2 of mean-field prediction. In contrast, the exponent with the RG transform is $\beta=0.175\pm0.018$. This value slightly deviates from the 1/8 of the 2D Ising model. The deviation may come from the gradually enlarged order parameter or the gradually enlarged film thickness. Nevertheless, the result show that the 2D Ising-type criticality can be traced by

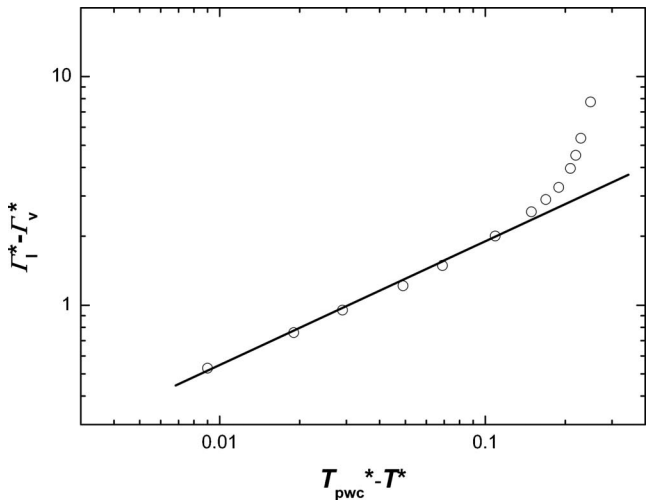

FIG. 3. Determination of the critical exponent β for prewetting without the confined RG transform. The symbols are the calculated results, and the solid lines are the best linear regressions of the first six points counting from the left side.

applying the confined RG transform to the DFT model.

Another characteristic of the system is the wetting temperature or the lower boundary of the prewetting transition. The wetting temperature can be determined with two different methods. First, it can be identified if the difference between the bulk and prewetting saturation chemical potentials $\Delta\mu^*=\mu_b^*-\mu_{pw}^*$ goes to zero. More over, Ancilotto and Toigo[14] suggested that the difference should scale as $\Delta\mu^* \propto (T^*-T_w^*)^{3/2}$ if the tail of the surface potential has a van der Waals tail, i.e., $\frac{C_{vdW}}{(z-z_{vdW})^3}$. Figure 5 shows $\Delta\mu^*$ as a function of temperature obtained with the RG transform. A fit to the function generates an estimate of $T_w^*=0.797$, or the real temperature $T_w=95.162$ K. On the other hand, the wetting temperature can be obtained by evaluating the contact angle for the given surface field with Young's equation, which is

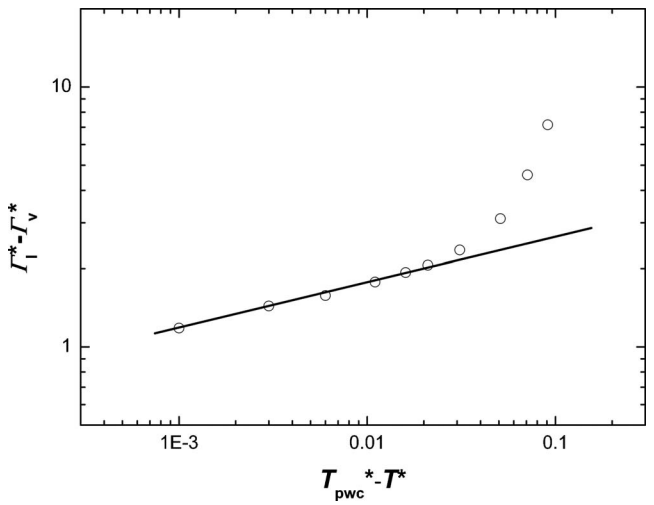

FIG. 4. Determination of the critical exponent β for prewetting with the confined RG transform. The symbols are the calculated results, and the solid lines are the best linear regressions of the first six points counting from the left side.

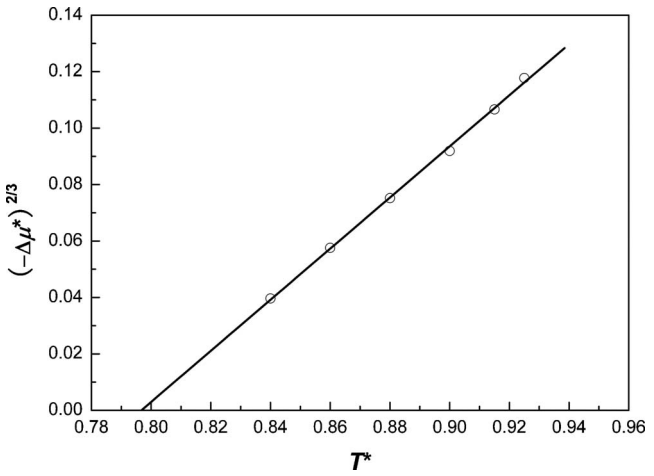

FIG. 5. Temperature dependence of the chemical potential difference $\Delta\mu^*=\mu_b^*-\mu_{pw}^*$. The solid line represents extrapolation to the wetting temperature.

known to very accurate when used to predict the contact angle in the case of wall-fluid systems.[43] The contact angle is determined by the surface tension balance and goes to zero as the wetting temperature is approached. Figure 6 presents the contact angle as a function of the temperature. The calculated results can be fitted with a line, showing a distinctive first-order wetting transition. The wetting temperature determined with $\cos\theta=1$ is $T_w^*=0.805$, corresponding to a real temperature $T_w=96.117$ K. Combining the results given by the two different methods, one can find that the agreement is quite accurate. The small discrepancy may be due to the influence of system size effects, which has been discussed by Grzelak and Errington recently.[44] In contrast, the DFT study by Sartarelli and Szybisz[20] obtained a higher wetting temperature with $T_w=110$ K. The quantitative difference can be attributed to the different treatment of attractive interactions. They used a mean-field approximation while we used an accurate direct correlation function[42] to account for the inhomogeneity.

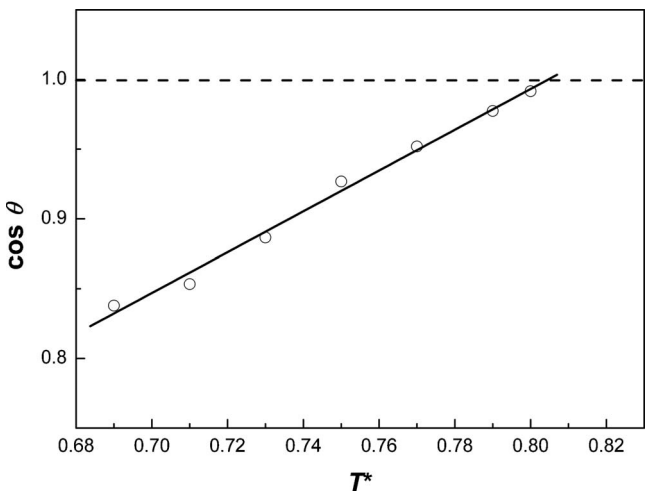

FIG. 6. Calculated contact angles as a function of temperature, where the wetting temperature T_w^* corresponds to $\cos\theta=1$. The solid line is a linear fitting of the symbols.

IV. CONCLUSIONS

In this work, the DFT was integrated with the RG theory to describe the behavior of Ar adsorbed on a planar structureless Li surface. The density profiles corresponding to the thin and thick films at prewetting coexistence were calculated. Unlike previous studies that ignore the 2D density fluctuations, we accounted for this issue by adopting the confined RG transform. Our calculation shows the thermodynamic consistency outside and inside the critical region. With the RG transform, the prewetting critical temperature is found to be lower than that of without the RG transform. By reproducing the critical exponent of 2D Ising universality, the method is validated to capture the features of prewetting transition within the critical region. The wetting temperature calculated by extrapolation of the chemical difference is in good agreement with the temperature from evaluation the contact angle via Young's equation. On the basis of the analysis of the prewetting critical temperature and the wetting temperature, we can conclude that the upper and lower boundaries of the prewetting transition of Ar on Li surface are reliable.

ACKNOWLEDGMENTS

This work is supported by Program for New Century Excellent Talents in University (NCET) of China, and the financial support of the National Natural Science Foundation of China (NNSFC) (Grants No. 20876007 and No. 20725622) is greatly appreciated.

*Author to whom correspondence should be addressed; mijg@mail.buct.edu.cn

[1] L. D. Gelb, K. E. Gubbins, R. Radhakrishman, and M. Sliwainska-Bartkowiak, Rep. Prog. Phys. **62**, 1573 (1999).
[2] R. Pandit, M. Schick, and M. Wortis, Phys. Rev. B **26**, 5112 (1982).
[3] J. W. Cahn, J. Chem. Phys. **66**, 3667 (1977).
[4] C. Ebner and W. F. Saam, Phys. Rev. Lett. **38**, 1486 (1977).
[5] J. E. Rutledge and P. Taborek, Phys. Rev. Lett. **69**, 937 (1992).
[6] G. Mistura, D. Reinelt, S. Herminghaus, P. Leiderer, and M. H. W. Chan, J. Low Temp. Phys. **101**, 211 (1995).
[7] M. Yao and F. Hensel, J. Phys.: Condens. Matter **8**, 9547 (1996).
[8] R. Evans and P. Tarazona, Phys. Rev. A **28**, 1864 (1983).
[9] E. Bruno, C. Caccamo, and P. Tarazona, Phys. Rev. A **35**, 1210 (1987).
[10] J. E. Finn and P. A. Monson, Phys. Rev. A **39**, 6402 (1989).
[11] E. Velasco and P. Tarazona, Phys. Rev. A **42**, 2454 (1990).
[12] Y. Fan and P. A. Monson, J. Chem. Phys. **99**, 6897 (1993).
[13] G. Mistura, F. Ancilotto, L. Bruschi, and F. Toigo, Phys. Rev. Lett. **82**, 795 (1999).
[14] F. Ancilotto and F. Toigo, Phys. Rev. B **60**, 9019 (1999).
[15] S. Curtarolo, G. Stan, M. J. Bojan, M. W. Cole, and W. A. Steele, Phys. Rev. E **61**, 1670 (2000).
[16] W. Shi, X. Zhao, and J. K. Johnson, Mol. Phys. **100**, 2139 (2002).
[17] J. R. Errington, Langmuir **20**, 3798 (2004).
[18] J. R. Errington and D. W. Wilbert, Phys. Rev. Lett. **95**, 226107 (2005).
[19] S. A. Sartarelli, L. Szybisz, and I. Urrutia, Phys. Rev. E **79**, 011603 (2009).
[20] S. A. Sartarelli and L. Szybisz, Phys. Rev. E **80**, 052602 (2009).
[21] F. Ancilotto, M. Barranco, E. S. Hernández, A. Hernando, and M. Pi, Phys. Rev. B **79**, 104514 (2009).
[22] M. S. Sellers and J. R. Errington, J. Phys. Chem. C **112**, 12905 (2008).
[23] W. F. Saam, J. Low Temp. Phys. **157**, 77 (2009).
[24] S. M. Gatica and M. W. Cole, J. Low Temp. Phys. **157**, 111 (2009).
[25] D. Y. Zhao, J. L. Feng, S. Q. Huo, N. Melosh, G. H. Fredrickson, B. F. Chmelka, and G. D. Stucky, Science **279**, 548 (1998).
[26] H. Nakanishi and M. E. Fisher, Phys. Rev. Lett. **49**, 1565 (1982).
[27] D. Nicolaides and R. Evans, Phys. Rev. Lett. **63**, 778 (1989).
[28] K. G. Wilson, Phys. Rev. B **4**, 3174 (1971); **4**, 3184 (1971).
[29] J. A. White and S. Zhang, J. Chem. Phys. **99**, 2012 (1993).
[30] M. Zeng, J. Mi, and C. Zhong, J. Phys. Chem. B **114**, 3894 (2010).
[31] Y. Yu and J. Wu, J. Chem. Phys. **116**, 7094 (2002).
[32] Y. Yu and J. Wu, J. Chem. Phys. **117**, 10156 (2002).
[33] J. A. Barker and D. Henderson, J. Chem. Phys. **47**, 2856 (1967).
[34] R. L. Cotterman, B. J. Schwarz, and J. M. Prausnitz, AIChE J. **32**, 1787 (1986).
[35] J. A. Barker, R. A. Fisher, and R. O. Watts, Mol. Phys. **21**, 657 (1971).
[36] A. Chizmeshya, M. W. Cole, and E. Zaremba, J. Low Temp. Phys. **110**, 677 (1998).
[37] S. C. Kim and S. H. Lee, J. Phys.: Condens. Matter **16**, 6365 (2004).
[38] J. K. Lee, J. A. Barker, and G. M. Pound, J. Chem. Phys. **60**, 1976 (1974).
[39] Y. Tang and B. C.-Y. Lu, Mol. Phys. **90**, 215 (1997).
[40] Y. Tang and B. C.-Y. Lu, AIChE J. **43**, 2215 (1997).
[41] E. Thiele, J. Chem. Phys. **39**, 474 (1963).
[42] M. Zeng, Y. Tang, J. Mi, and C. Zhong, J. Phys. Chem. C **113**, 17428 (2009).
[43] C. Bruin, M. J. P. Nijmeijer, and R. M. Crevecoeur, J. Chem. Phys. **102**, 7622 (1995).
[44] E. M. Grzelak and J. R. Errington, J. Chem. Phys. **132**, 224702 (2010).